Synthesis and Evaluation of Bisbenzylidenedioxotetrahydrothiopranones as Activators of Endoplasmic Reticulum (ER) Stress Signaling Pathways and Apoptotic Cell Death in Acute Promyelocytic Leukemic Cells

Kheng-Lin Tan,[†] Azhar Ali,[‡] Yuhong Du,[§] Hainan Fu,[§] Hai-Xiao Jin,[∥] Tan-Min Chin,[‡] Matiullah Khan,[⊥] and Mei-Lin Go*,[†]

[†]Department of Pharmacy, National University of Singapore, 18 Science Drive 4, 117543, Republic of Singapore

[‡]Cancer Science Institute of Singapore, Yong Loo Lin School of Medicine, National University of Singapore, 10 Medical Drive, 117597, Republic of Singapore

[§]Department of Pharmacology, Emory Chemical Biology Discovery Centre, Emory University School of Medicine, 1462 Clifton Road, Atlanta, Georgia 30322, United States

[∥]Key Laboratory of Applied Marine Biotechnology, Ministry of Education, School of Marine Sciences, Ningbo University, Fenghua Road 818, Jiangbei District, Ningbo, Zhejiang 315211, People's Republic of China

[⊥]School of Medicine, Asian Institute of Medicine, Science and Technology (AIMST), Jalan Bedong Semeling, 08100, Bedong, Kedah, Malaysia

S Supporting Information

ABSTRACT: Curcumin is known to trigger ER-stress induced cell death of acute promyelocytic leukemic (APL) cells by intercepting the degradation of nuclear co-repressor (N-CoR) protein which has a key role in the pathogenesis of APL. Replacing the heptadienedione moiety of curcumin with a monocarbonyl cross-conjugated dienone embedded in a tetrahydrothiopyranone dioxide ring resulted in thiopyranone dioxides that were more resilient to hydrolysis and had greater growth inhibitory activities than curcumin on APL cells. Several members intercepted the degradation of misfolded N-CoR and triggered the signaling cascade in the unfolded protein response (UPR) which led to apoptotic cell death. Microarray analysis showed that genes involved in protein processing pathways that were germane to the activation of the UPR were preferentially up-regulated in treated APL cells, supporting the notion that the UPR was a consequential mechanistic pathway affected by thiopyranone dioxides. The Michael acceptor reactivity of the scaffold may have a role in exacerbating ER stress in APL cells.
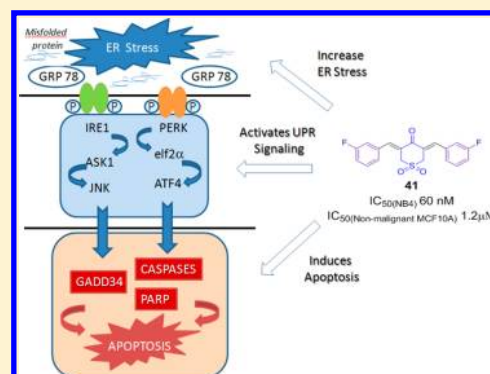
1. INTRODUCTION

Acute promyelocytic leukemia (APL) is caused by the fusion protein PML-RARα that is formed by the reciprocal translocation of *PML* and *RARα* genes located at chromosomes 15 and 17.[1,2] The oncogenic potential of the PML-RARα fusion protein is linked to the nuclear receptor co-repressor (N-CoR) protein,[3−6] which is recruited by the fusion protein to give the N-CoR-PML-RARα complex. The latter represses retinoic acid responsive genes that are essential for the maturation of promyelocytic cells, hence curtailing cell differentiation and transformation.[7,8] The PML-RARα fusion protein also induces misfolding of N-CoR which leads to increased levels of endoplasmic reticulum (ER) stress due to the accumulation of misfolded protein.[9] In an effort to restore ER homeostasis, cells activate the unfolded protein response (UPR) which entails temporarily shutting down protein translation and up-regulating ER folding and quality control mechanisms.[10,11] In APL cells, this is achieved in part by protease-mediated and ER-associated degradation (ERAD) of misfolded N-CoR.[12−14] If ER stress persists, the UPR shifts to a prodeath mode in an effort to eliminate cells harboring deleterious malfolded proteins.[10,11,15] Curcumin, the active substance of the spice turmeric (*Curcuma longa*), was reported to block the protease- and proteasomal-mediated degradation of N-CoR.[16] The resulting build-up of misfolded N-CoR amplified ER stress and caused the UPR to switch from a prosurvival to a proapoptotic mode. ER stress-induced apoptosis is increasingly viewed as an attractive and novel signaling target for anticancer therapies,[11,17] and the ability of curcumin to sensitize APL[16] and other malignant cells[18−21] to apoptosis underscores its anticancer potential. There are however several shortcomings to curcumin that has limited its therapeutic usefulness, notably its modest potency, intrinsic instability, and limited bioavailability.[22,23]
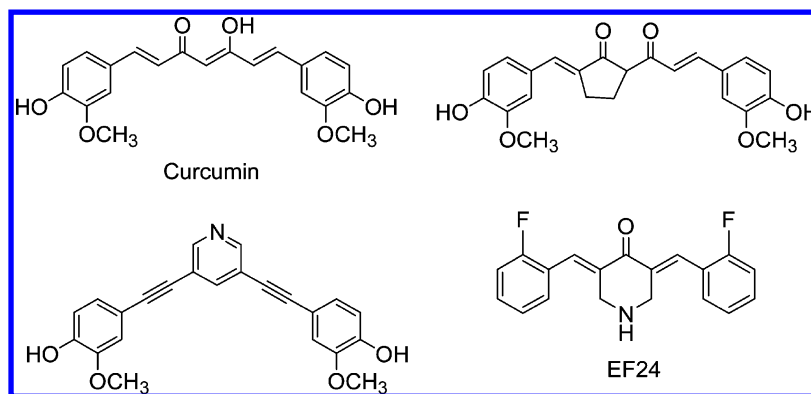
Figure 1. Structures of curcumin and representative analogues designed to address the activity and pharmacokinetic limitations of curcumin.[25,26]
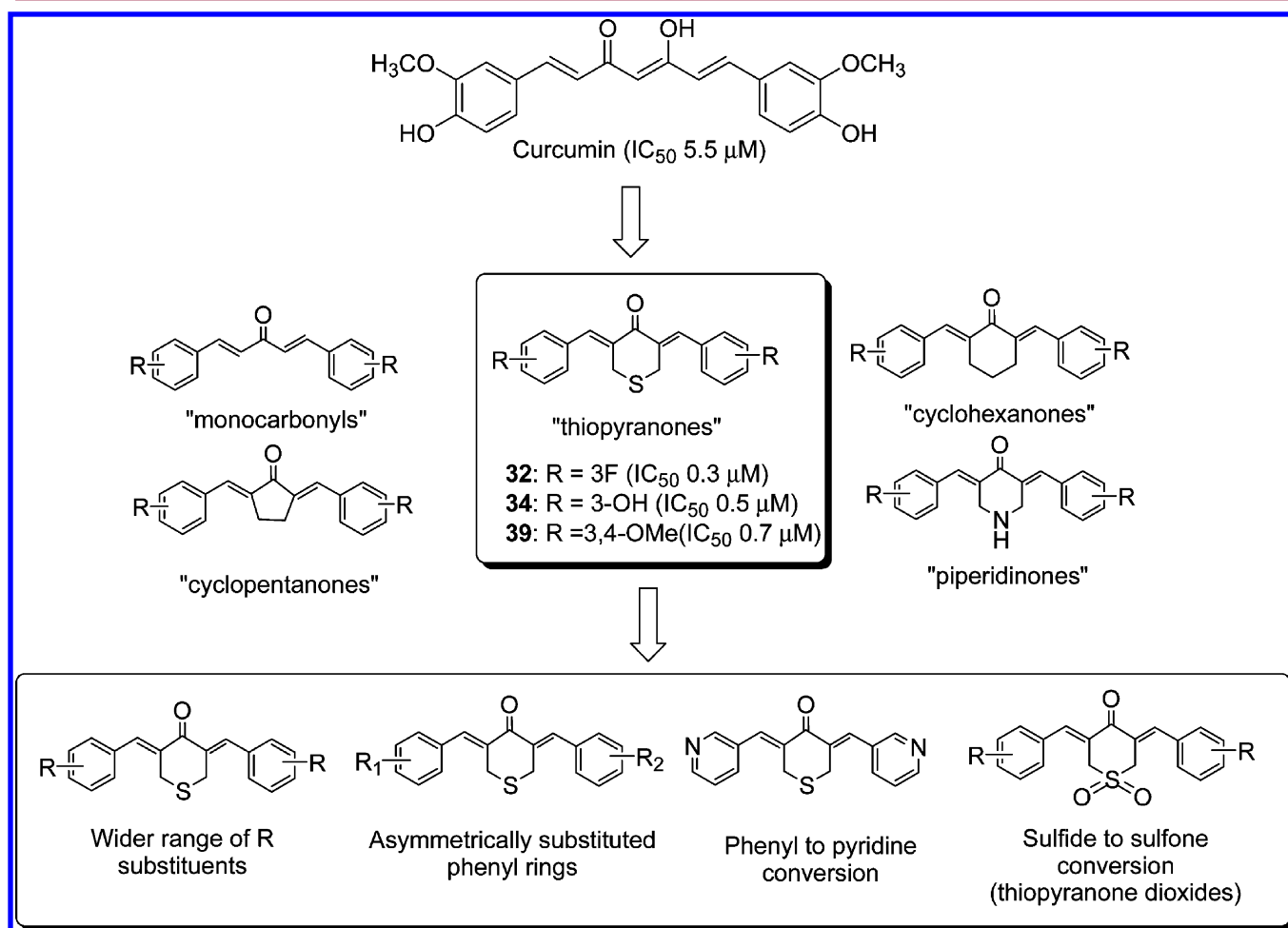
Figure 2. Replacement of the β-diketone moiety of curcumin by monocarbonyl cross-conjugated dienones (monocarbonyls, cyclopentanones, cyclohexanones, thiopyranones, piperidinones). The thiopyranones **32**, **34**, and **39** had potent growth inhibitory activities (IC$_{50}$) on NB4, an APL cell line,[27] and were targeted for further modifications (shown in box) in this report.

Various strategies have been proposed to address these limitations such as engaging novel formulations to enhance delivery of curcumin[22,24] and modifying the curcumin scaffold to improve pharmacokinetic and potency end points.[25,26] Some examples are provided in Figure 1. We had previously investigated the APL growth inhibitory activity of compounds derived by replacing the conjugated β-diketone moiety of curcumin with a monocarbonyl cross-conjugated dienone that was either unmodified ("monocarbonyls") or embedded in carbocyclic ("cyclopentanones", "cyclohexanones") or heterocyclic

("thiopyranones", "piperidinones") rings (Figure 2).[27] Several compounds bearing the tetrahydrothiopyran ring ("thiopyranones") were found to arrest APL cell proliferation at lower concentrations (IC$_{50}$ = 0.3–1 μM) than curcumin (IC$_{50}$ = 5.5 μM). To further explore the potential of this scaffold, additional structural modifications were investigated in this report, namely, asymmetrical substitution of the terminal phenyl rings, switching of the latter to pyridine, and replacement of the thiopyranone ring with thiopyranone 1,1-dioxide (Figure 2). Herein we describe the synthesis and growth inhibitory properties of these compounds

on APL cells, the hydrolytic stabilities of selected members, and in view of their structural connection to curcumin, the involvement of ER stress-induced apoptosis in the mechanistic pathways of potent members. In addition, the effects of a representative potent member (41) on the expression of genes involved in ER protein processing and on selected proteins/transcription factors that mediate the response to ER stress in the UPR signaling pathway were examined for mechanistic insight.

2. RESULTS

2.1. Chemistry. In a previous report, thiopyranones 32, 34, 39 (Figure 2) were found to be potent inhibitors of APL cell viability.[27] Their antiproliferative activities were broadly comparable to their piperidinone counterparts but exceeded that of the monocarbonyl, cyclopentanone, and cyclohexanone analogues. Unlike the piperidinones which have been intensively investigated for their anticancer and anti-inflammatory activities,[28−31] less is known of the structure−activity relationship or mechanistic profile of thiopyranones. Hence, to appropriate the full potential of this scaffold, we undertook the following modifications. First, fluoro, hydroxyl, and/or methoxy groups were introduced at various positions on the terminal rings. As shown in Figure 2, these groups were present in the earlier hits 32, 34, and 39.[27] Second, asymmetric substitution of the phenyl rings was explored with the above-mentioned groups. Third, the phenyl rings were replaced by pyridines, motivated in part by the good results observed for several cyclohexanones[27] and piperidinones[28] which had similar phenyl-to-pyridine substitution. Lastly, the thiopyranone ring was replaced by thiopyranone 1,1-dioxide. Table 1 lists the compounds synthesized in this report. Besides the thiopyranones (series I) and thiopyranone dioxides (series II), several cyclohexanones (series III) and piperidinones (series IV) were also prepared for comparison to their sulfur-containing counterparts in series I and II.

Series I, III, and IV compounds that have symmetrically substituted phenyl rings were obtained in good yields by a base-catalyzed aldol condensation reaction between the ketone (cyclohexanone, tetrahydrothiopyranone, piperidinone) and an arylcarboxaldehyde (Scheme 1A). In the case of benzaldehydes with phenolic hydroxyl groups, no hydroxyl protection was required when aldol condensation with the ketone (tetrahydrothiopyranone, piperidinone) was carried out under acidic conditions. The final products (215, 216, 230, 231) were obtained in reasonably good yields (24−60%). Oxidation of the thiopyranone sulfide with 30% hydrogen peroxide in acetic acid gave the corresponding thiopyranone 1,1-dioxides of series II (Scheme 1A).

The asymmetrically substituted cyclohexanones (202−205) and thiopyranones (217−220) were prepared sequentially by reacting the ketone with 3-fluorobenzaldehyde to give intermediates (1, 2) which were then reacted in a second aldol condensation under acidic conditions with the methoxy/hydroxyl substituted benzaldehyde. The intermediate 2-(3-fluorobenzylidene)cyclohexanone (1) was obtained under acidic conditions in the presence of a large excess of cyclohexanone (Scheme 1B), but strong basic conditions were required for the synthesis of intermediate 2 ((3-fluorobenzylidene)dihydro-2*H*-thiopyran-4(3*H*)-one, Scheme 1C). To obtain 2, dihydro-2*H*-thiopyran-4(3*H*)-one was reacted with lithium diisopropylamide (LDA) at low temperatures to generate the nucleophilic enolate which attacked the electrophilic carbonyl carbon of 3-fluorobenzaldehyde to give the hydroxyl intermediate on aqueous workup. The latter

was dehydrated in the presence of *p*-toluenesulfonic acid to give 2 (21% isolated yield). Acid-catalyzed aldol condensation of 2 and the methoxy or hydroxyl substituted benzaldehyde gave the desired thiopyranones 217−220.

2.2. Growth Inhibitory Activities of Curcumin Analogues on APL Cell Lines. The test compounds were evaluated on two APL cell lines, NB4 and NB4-R1. NB4 cells respond to retinoic acid which is the standard treatment for APL,[32] whereas NB4-R1, a de novo cell line derived from parental NB4 cells,[33] is retinoic acid resistant. Table 1 lists the growth inhibitory IC_{50} values (concentration required to reduce cell viability to 50% of levels observed in untreated cells after 72 h of exposure) of the test compounds on these cell lines. Also included in Table 1 are previously determined IC_{50} values of selected thiopyranones, cyclohexanones, and piperidinones.[27]

The most potent thiopyranones in Table 1 were 207 (IC_{50} = 0.17 μM) and 208 (IC_{50} = 0.11 μM) which have pyridine in place of phenyl as terminal rings. Their growth inhibitory activities surpassed that of 32 (IC_{50} = 0.29 μM) which was the most potent thiopyranone identified earlier.[27] Interestingly, the growth inhibitory activities of 207 and 208 were comparable to that of the potent cyclohexanones 24 (0.19 μM) and 25 (IC_{50} = 0.22 μM) which also have terminal pyridines. Furthermore, a recent report highlighted potent kinase inhibition by a piperidinone analogue with terminal 2-pyridinyl rings.[28] Thus, there is anecdotal support for the activity-enhancing potential of a phenyl to pyridine substitution across various carbonyl cross-conjugated dienone scaffolds related to curcumin.

A comparison of the growth inhibitory activities of thiopyranones and cyclohexanones revealed interesting scaffold-dependent differences in the structure−activity relationship (SAR). Notably, a regioisomeric preference was observed among the pyridine-bearing thiopyranones that was not apparent among the cyclohexanone counterparts (24−26). For instance, thiopyranone 209 with 4-pyridinyl rings was less active than its 2- or 3-pyridinyl counterparts, a distinction that was not seen among the pyridine-bearing cyclohexanones. Additionally, methoxy substitution of the pyridine ring was well tolerated in the thiopyranone 210 (IC_{50} = 0.17 μM versus unsubstituted 208 IC_{50} = 0.11 μM) but not in the cyclohexanone 201 (IC_{50} = 1.06 μM versus unsubstituted 25 IC_{50} = 0.22 μM).

The presence of hydroxyl/methoxy groups in the hit compounds 34 and 39 prompted us to investigate more of such thiopyranones (211, 213−216), but disappointingly, only incremental improvements in activity were observed. Notably, the most promising thiopyranone 215 (R = 3-OH, 4-OCH$_3$; IC_{50} = 0.38 μM) was marginally more active than the original hits 34 and 39. On the other hand, dimethoxy and trimethoxy substitution resulted in exceptionally poor activities as seen from 213 (2,5-OCH$_3$, IC_{50} = 3.23 μM) and 214 (3,4,5-OCH$_3$, IC_{50} = 3.82 μM). The contrasting activities of 213 and its 3,4-regioisomer 39 were striking and pointed to a preference for certain substitution patterns on the terminal rings. Again, scaffold-dependent SAR was apparent as piperidinones bearing the same dimethoxy/trimethoxy (228, 229) groups retained outstanding submicromolar activities. In fact, the trimethoxy substituted piperidinone 229 (IC_{50} = 0.10 μM) was the most potent member in its class.
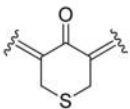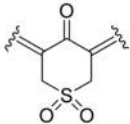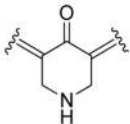
For thiopyranones with asymmetrically substituted phenyl rings in which 3-fluoro was retained on one phenyl ring and hydroxyl/methoxy groups on the other ring, no apparent advantage was observed among the asymmetrically substituted analogues (217−220) vis-à-vis their symmetrically substituted

Table 1. Mean Growth Inhibitory Activity (IC$_{50}$, μM) of Compounds on Two Human APL Cell Lines

Compound		Substituents (R$_1$, R$_2$)[b]	Mean IC$_{50}$ (μM) ± SD[a]	
Ref name	Linker		NB4[c]	NB4-R1[c]
Curcumin		3-OCH$_3$, 4-OH	6.01 ± 1.91	7.99 ± 1.02
13[d]		2-F	N.D.[e]	>5[f]
14[d]		3-F	1.67 ± 0.26	2.53 ± 0.08
15[d]		4-F	N.D.[e]	>5[f]
16[d]		3-OH	0.98 ± 0.06	1.68 ± 0.65
21[d]		3-OCH$_3$, 4-OCH$_3$	5.57 ± 2.01	5.85 ± 0.09
24[d]		2-Py[g]	0.19 ± 0.03	0.24 ± 0.02
25[d]		3-Py[g]	0.22 ± 0.02	0.43 ± 0.14
26[d]		4-Py[g]	0.27 ± 0.04	0.43 ± 0.08
201		3-Py-5-OCH$_3$, 6-OCH$_3$	1.06 ± 0.10	1.01 ± 0.21
202		R$_1$ = 3-F, R$_2$ = 3-OCH$_3$, 4-OCH$_3$	3.89 ± 0.96	3.89 ± 0.66
203		R$_1$ = 3-F, R$_2$ = 3-OH,4-OH	1.37 ± 0.23	1.19 ± 0.09
204		R$_1$ = 3-F, R$_2$ = 3-OH,4-OCH$_3$	1.75 ± 0.35	1.86 ± 0.18
205		R$_1$ = 3-F, R$_2$ = 3-OH	1.42 ± 0.36	1.17 ± 0.15
206		3-F, 4-OCH$_3$	5.35 ± 1.02	6.82 ± 1.12
31[d]		2-F	0.94 ± 0.21	1.09 ± 0.06
32[d]		3-F	0.29 ± 0.11	0.66 ± 0.03
33[d]		4-F	1.07 ± 0.24	1.54 ± 0.45
34[d]		3-OH	0.51 ± 0.07	0.59 ± 0.34
39/212[d]		3-OCH$_3$, 4-OCH$_3$	0.69 ± 0.13	0.52 ± 0.15
207		2-Py[g]	0.17 ± 0.04	0.10 ± 0.02
208		3-Py[g]	0.11 ± 0.02	0.11 ± 0.01
209		4-Py[g]	>40[h]	>40[h]
210		3-Py-5-OCH$_3$, 6-OCH$_3$	0.17 ± 0.02	0.27 ± 0.09

Table 1. continued

Compound		Substituents (R_1, R_2)[b]	Mean IC_{50} (μM) $\pm$ SD[a]	
Ref name	Linker		NB4[c]	NB4-R1[c]
211		3-F, 4-OCH$_3$	5.42 $\pm$ 1.88	5.69 $\pm$ 1.20
213		2-OCH$_3$, 5-OCH$_3$	3.23 $\pm$ 0.63	1.79 $\pm$ 0.36
214		3-OCH$_3$, 4-OCH$_3$, 5-OCH$_3$	3.82 $\pm$ 1.38	0.16 $\pm$ 0.02
215		3-OH, 4-OCH$_3$	0.38 $\pm$ 0.04	0.33 $\pm$ 0.09
216		3-OCH$_3$, 4-OH	0.84 $\pm$ 0.27	0.58 $\pm$ 0.16
217		R_1 = 3-F, R_2 = 3-OCH$_3$, 4-OCH$_3$	0.94 $\pm$ 0.15	0.56 $\pm$ 0.24
218		R_1 = 3-F, R_2 = 3-OH,4-OH	0.90 $\pm$ 0.16	0.55 $\pm$ 0.13
219		R_1 = 3-F, R_2 = 3-OH,4-OCH$_3$	0.48 $\pm$ 0.12	0.21 $\pm$ 0.07
220		R_1 = 3-F, R_2 = 3-OH	0.41 $\pm$ 0.03	0.24 $\pm$ 0.10
40		2-F	0.08 $\pm$ 0.02	0.07 $\pm$ 0.00
41		3-F	0.06 $\pm$ 0.02	0.07 $\pm$ 0.01
221		4-F	0.05 $\pm$ 0.01	0.11 $\pm$ 0.04
222		3-OCH$_3$, 4-OCH$_3$	0.12 $\pm$ 0.02	0.10 $\pm$ 0.03
223		2-OCH$_3$, 5-OCH$_3$	0.29 $\pm$ 0.09	0.23 $\pm$ 0.07
224		3-OCH$_3$, 4-OCH$_3$, 5-OCH$_3$	0.05 $\pm$ 0.01	0.04 $\pm$ 0.01
225		3-OH, 4-OCH$_3$	0.17 $\pm$ 0.04	0.15 $\pm$ 0.04
226		3-OH	0.14 $\pm$ 0.02	0.16 $\pm$ 0.03
227		3-F, 4-OCH$_3$	0.08 $\pm$ 0.01	0.08 $\pm$ 0.00
42[d]		2-F	0.29 $\pm$ 0.05	0.32 $\pm$ 0.05
43[d]		3-F	0.16 $\pm$ 0.04	0.21 $\pm$ 0.00
44[d]		4-F	0.25 $\pm$ 0.02	0.36 $\pm$ 0.08
45[d]		3-OH	0.20 $\pm$ 0.08	0.44 $\pm$ 0.21
47[d]		3-OCH$_3$, 4-OCH$_3$	0.50 $\pm$ 0.02	0.80 $\pm$ 0.20
228		2-OCH$_3$, 5-OCH$_3$	0.34 $\pm$ 0.06	0.24 $\pm$ 0.03
229		3-OCH$_3$, 4-OCH$_3$, 5-OCH$_3$	0.10 $\pm$ 0.03	0.10 $\pm$ 0.01
230		3-OH, 4-OCH$_3$	0.39 $\pm$ 0.07	0.42 $\pm$ 0.08
231		3-OCH$_3$, 4-OH	0.40 $\pm$ 0.09	0.57 $\pm$ 0.16

[a]Concentration required to effect 50% inhibition of cell growth. Results are the mean $\pm$ standard deviation of at least three independent experiments. [b]R_1 = R_2 unless indicated otherwise. [c]APL cell lines. NB4 is sensitive to retinoic acid. NB4-R1 is resistant to retinoic acid. [d]IC_{50} values were previously reported.[27] [e]Not determined. [f]IC_{50} not determined above 5 μM. [g]Phenyl replaced by pyridine (Py). [h]IC_{50} not determined above 40 μM because of solubility issues.

counterparts (**32, 34, 39, 215**). A similar trend was observed for the asymmetrically substituted cyclohexanones (**202−205**).

Oxidation of the thiopyranone sulfide to sulfone gave rise to a series of thiopyranone dioxides (**40, 41, 221−227**). Here, we

E

dx.doi.org/10.1021/jm401352a | J. Med. Chem. XXXX, XXX, XXX−XXX
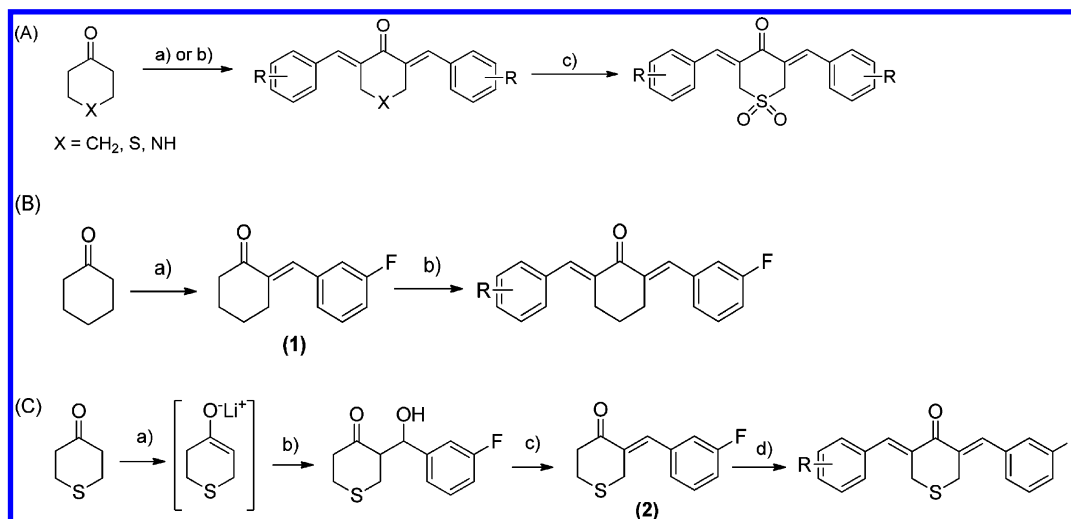
Scheme 1[a]

[a](A) Synthesis of selected series I−III analogues, reagents and conditions: (a) substituted benzaldehyde or pyridinecarboxaldehyde (2.1 equiv), NaOH (3 equiv), EtOH, 25 °C, 18−24 h; (b) substituted benzaldehyde (2.1 equiv), conc HCl, EtOH, 60 °C, 18−24 h; (c) For X = S: 30% H_2O_2, CH_3COOH, 60 °C, 6−24 h. (B) Synthesis of asymmetrical series III analogues **203−205**, reagents and conditions: (a) 3-fluorobenzaldehyde (2.1 equiv), conc HCl, EtOH, 60 °C, 18−24 h; (b) substituted benzaldehyde (2.1 equiv), conc HCl, EtOH, 60 °C, 18−24 h. (C) Synthesis of asymmetrical series I analogues **217−220**, reagents and conditions: (a) LDA (2 M), dry THF, −78 °C, 1 h; (b) 3-fluorobenzaldehyde (1 equiv), dry THF, −78 °C, 6 h; (c) p-TsOH (5 mol %), toluene, 90 °C, 1.5 h; (d) substituted benzaldehyde (1 equiv), conc HCl, EtOH, 60 °C, 18−24 h.

found potent nanomolar activities among the fluoro substituted analogues **40**, **41**, **221** (IC$_{50}$ = 0.05−0.08 μM), the trimethoxy analogue **224** (IC$_{50}$ = 0.05 μM), and the 3-fluoro-4-methoxy analogue **227** (IC$_{50}$ = 0.08 μM). When compared with cyclohexanones, thiopyranones, and piperidinones bearing similar ring substituents, the thiopyranone dioxide analogue was clearly superior in terms of growth inhibitory activity. Notably, **41** and **224** were nearly twice as potent as their piperidinone counterparts (**43** and **229**), and **227** far exceeded cyclohexanone **206** and thiopyranone **211** (IC$_{50}$ ≈ 5 μM) which have the same ring substituents.

We then considered the antiproliferative activities of the test compounds on the retinoic acid resistant NB4-R1 cell line. Curcumin was equipotent on both NB4 (IC$_{50}$ = 6 μM) and NB4-R1 (IC$_{50}$ = 8 μM) cells, and this was also observed for most of the compounds listed in Table 1. A notable exception was the trimethoxy-substituted thiopyranone **214**, which was at least 20 times more potent on NB4-R1 (IC$_{50}$ = 0.16 μM) than NB4 (IC$_{50}$ = 3.82 μM). Otherwise, SAR trends were generally similar to those observed on the retinoic acid sensitive NB4 cells.

2.3. Hydrolytic Stabilities of Thiopyranone Dioxides 41 and 227 and Thiopyranone 219. Liang and co-workers reported that replacing the conjugated diketone linker of curcumin with a monocarbonyl dienone moiety resulted in analogues with improved hydrolytic stabilities.[34] They investigated compounds that were structurally related, but not identical, to those investigated in this report and found that generally for the same substitution on the terminal phenyl rings, stabilities were of order cyclopentanones (most stable) > cyclohexanones > monocarbonyls (least stable). As thiopyranones and thiopyranone dioxides had shown good growth inhibitory activities (Table 1), we proceeded to assess their hydrolytic stabilities vis-à-vis curcumin. Hence, the stabilities of representative members (**41**, **219**, **227**) were determined at pH 7.4, 25 °C over 75 h. We found substantial time-dependent

degradation of curcumin (>90% after 75 h). Thiopyranone **219** and thiopyranone dioxides **41**, **227** were hydrolytically more stable but degraded over time, albeit to a lesser extent than curcumin. Thiopyranone dioxide **227** was initially more resistant to hydrolysis than **41** and **219** but after 75 h, all 3 compounds had broadly comparable levels of degradation (60−68%) (Supporting Information, Figure S1)

2.4. Thiopyranone Dioxide 41 and Related Compounds (219, 227) Induce Apoptotic Cell Death in NB4 Cells. Next, we went on to determine if the potent analogues **41**, **219**, and **227** induced apoptotic cell death. The compounds were incubated with NB4 cells for 48 h at their IC$_{50}$ $_{NB4}$ and higher concentrations, after which levels of cleaved caspases 3 and 9 and PARP were probed by Western blotting (Supporting Information, Figure S2). **41** and **219** induced dose dependent increases in cleaved caspase 9 levels at concentrations ranging from 1 × IC$_{50}$ to 5 × IC$_{50}$. In contrast, **227** did not activate caspase 9 even at 10 × IC$_{50}$. As cleavage of caspase 9 is initiated by the release of cytochrome c from the mitochondria in the intrinsic apoptotic pathway, this pathway may not be involved in **227**-induced apoptosis. All three compounds promoted the cleavage of the downstream executioner caspase 3 which was common to both intrinsic and extrinsic apoptotic pathways. Levels of cleaved PARP were also elevated. The induction of apoptotic cell death was further confirmed for **41** and **219** by FACS analysis of NB4 cells double stained with annexin V and propidium iodide (Figure S2).

2.5. Thiopyranone Dioxide 41 Induce Accumulation of N-CoR Protein in NB4 Cells. The accumulation of misfolded N-CoR is an incipient event leading to ER stress amplification and NB4 cell death.[9,12] Corroboratory evidence was adduced from curcumin which sensitized NB4 cells to ER stress induced apoptosis by blocking the loss of misfolded N-CoR[16] and structurally related monocarbonyl dienone analogues where accumulation of misfolded and nonfunctional N-CoR was cited as a basis of selective activity on NB4 cells.[27]
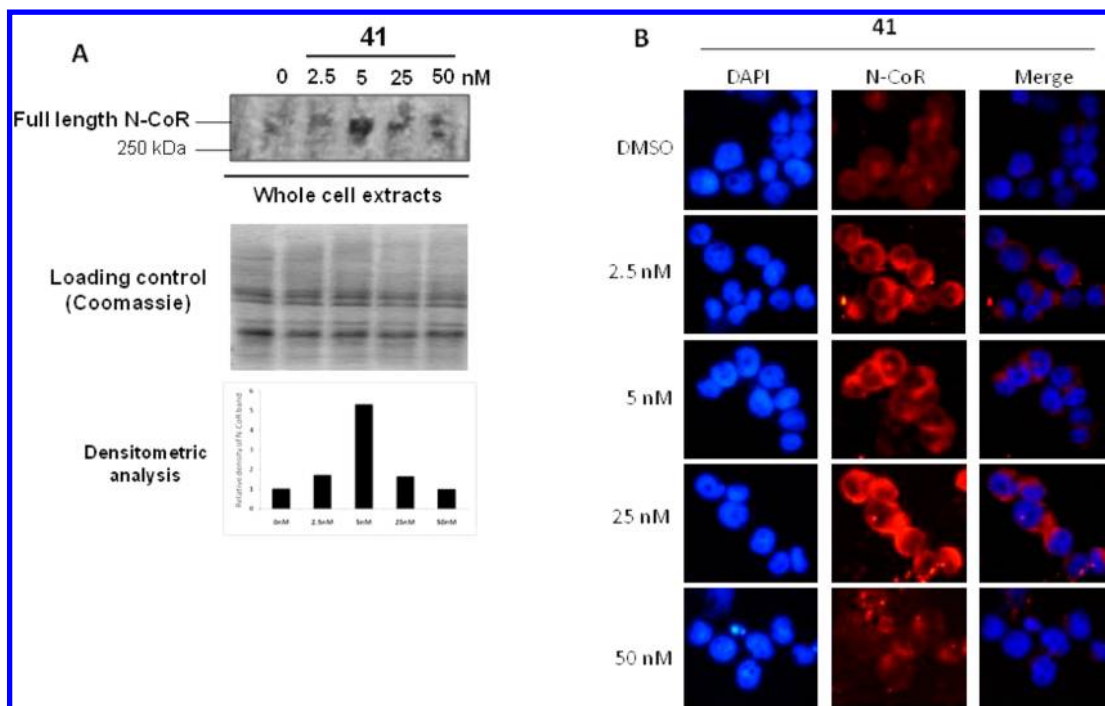
Figure 3. Thiopyranone dioxide **41** induced accumulation of misfolded N-CoR in NB4 cells. NB4 cells were treated for 48 h with test compound. (A) N-CoR protein levels in whole cell extracts were probed by Western blotting using anti-N-CoR antibody. Protein loading in each lane was monitored with coomassie stain. **41** increased N-CoR levels at 2.5, 5.0, and 25 nM. (B) Vehicle control comprises media with 0.5% DMSO. Cells were stained with DAPI to visualize cell nucleus (blue, left panel) and anti-N-CoR antibody to visualize N-CoR (red, middle panel). Localization of N-CoR in cytosol was shown by red ring around a blue core. Cytosolic N-CoR was detected in cells treated with **41** at 2.5 nM to 25 nM. Experiments were repeated at least twice for each compound at stated concentrations.

Having shown that thiopyranone dioxide **41** potently induced apoptosis, we proceeded to assess the involvement of N-CoR in the death process. NB4 cells were treated with **41** for 48 h, after which levels of N-CoR were probed by Western blotting. Control cells showed a faint band corresponding to low basal levels of full length N-CoR (Figure 3A) which corroborated earlier findings that N-CoR was predominantly fragmented in NB4 cells, with only a small proportion present in the intact folded or misfolded state which constituted full-length N-CoR.[12] Treatment with **41** at 5 nM intensified this band but with poor dose dependency. For further confirmation, we turned to in vitro immunofluorescence imaging to determine if the full length N-CoR was localized in the nucleus or cytosol. Only natively folded N-CoR was localized in the nucleus, whereas misfolded N-CoR was predominantly cytosolic.[12] In this method, N-CoR was detected by its antibody which gave a red fluorescence. When present in the nucleus, N-CoR had a purplish hue due to the merging of blue DAPI and red N-CoR images. Figure 3B shows muted red fluorescence in control NB4 cells, in keeping with low basal levels of N-CoR in these cells. When exposed to **41** (2.5 nM to 25 nM), the red N-CoR fluorescence intensified, signifying an increase in N-CoR levels. The increases were localized in the cytosol as seen from the red rings that surrounded the DAPI-stained (blue) nuclei (merged panel) which implied that most of the accumulated N-CoR induced by **41** was cytosolic and misfolded.

2.6. Thiopyranone Dioxide 41 and Related Compounds (219, 227) Activate the Unfolded Protein Response (UPR) in NB4 Cells. Next, we queried if the accumulation of misfolded N-CoR by **41** would amplify ER stress in NB4 cells. The UPR signaling pathway is mediated by ER stress sensors which are maintained in inactive states in nonstressed situations by chaperone proteins. In the presence of ER stress, these chaperones are released from the ER stress sensors for binding to misfolded proteins. The liberated ER stress sensors would then trigger UPR signaling pathways. Thus, levels of ER stress chaperone proteins PDI, GRP78, and HSP90 were probed by Western blotting in NB4 cells treated with **41**, **219**, and **227** (Supporting Information, Figure S3). All three compounds increased PDI, GRP78, and HSP60 levels, with **41** more potent than **219** and **227**. In the case of **41**, increases were evident at 250 nM compared to 2.5 μM (**219**) and 1 μM (**227**) respectively (Figure S3A).

Having shown that **41**, **219**, and **227** amplified ER stress in NB4 cells, we proceeded to investigate their effects on the ER stress sensors that mediate UPR signaling. These sensors (PERK, IRE1, and ATF6) are involved in both prosurvival and prodeath functions.[10,11,15] The switch from the initial prosurvival to the late prodeath response is determined in part by the relative stabilities of the mRNAs/proteins involved in the signaling pathways and the persistence of the ER stress.[10] Here, we determined levels of selected proteins recruited by PERK and IRE1 in NB4 cells treated with **41**, **219**, and **227** at their growth inhibitory $IC_{50\ NB4}$ for 24 and 48 h. PERK is activated early in the UPR and blocks general protein synthesis by phosphorylating elF2α. Persistent ER stress would direct signaling along the PERK-elF2α-ATF4 arm toward apoptotic cell death. Commitment to apoptosis is also relayed by dephosphorylation of elF2α by GADD34, a proapoptotic protein, thereby reversing the elF2α-induced block on translation. Time-dependent increases in phosphorylated PERK, phosphorylated elF2α, and GADD34 were observed in treated NB4 cells (Figure S3B).
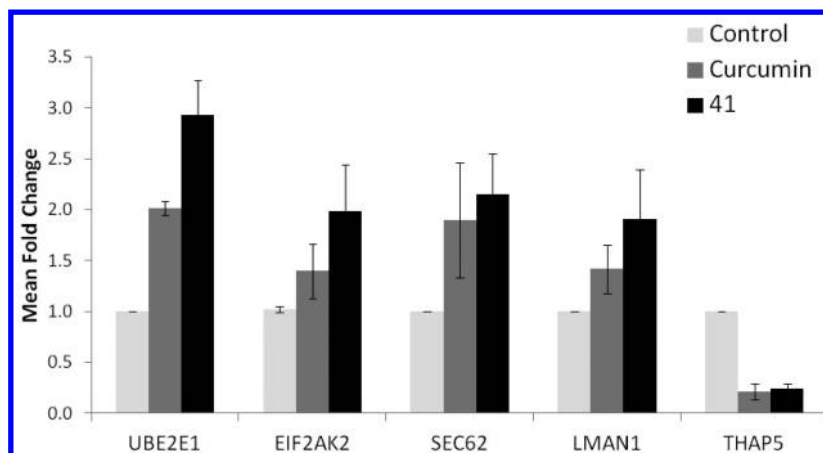
Figure 4. Validation of selected genes that were up- or down-regulated by **41** (50 nM) or curcumin (0.5 μM) by quantitative real-time PCR analysis. NB4 cells were treated with vehicle (0.1% DMSO), curcumin (5 μM), or **41** (50 nM) for 48 h. Real-time PCR was carried out to measure gene expression levels in treated samples. Changes in expression levels were compared to levels in control cells (normalized to 1) and presented as mean fold change relative to control. Results are the mean and SD of three independent experiments.

The IRE1 pathway is the final arm of the UPR and plays an important role in initiating proapoptotic signals. Initially, IRE1 aids cell survival by up-regulating the expression of ER stress chaperone proteins and genes involved in protein degradation, but if ER stress persists, IRE1 triggers apoptosis by recruiting ASK1 and JNK. Here, we monitored ASK1 and JNK (p54, p46) levels and observed increases in the phosphorylated states of both proteins in **219**- and **227**-treated cells (Figure S3C). We noted that **41** up-regulated phosphorylated ASK1 but did not increase phosphorylated JNK at the time points investigated. Taken together, we have shown that the test compounds activated ER chaperone proteins, caused sustained signaling in the PERK and IRE1 arms of the UPR, and activated downstream molecules (GADD34, ASK1, JNK) that were involved in relaying the proapoptotic signals to the final execution phase.

2.7. Thiopyranone Dioxide 41 Induces Expression of Genes Involved in Protein Processing in the Endoplasmic Reticulum. Curcumin is known to act on several protein targets,[25,35] and **41** which is structurally related to curcumin may be similarly disposed to a pleiotropic profile. If the latter is true, we would then have to ask if ER stress and UPR signaling are the main triggers of **41**-induced apoptotic cell death which is central to our hypothesis. Hence, we monitored the gene expression profile of NB4 cells treated with **41** at its IC$_{50 \text{ NB4}}$ concentration of 50 nM for 48 h. Analysis of the results revealed that 599 genes were significantly altered by 2-fold or more (adjusted p value of <0.05) in **41**-treated cells, with most genes (581) up-regulated. KEGG pathway analysis of the microarray profiles identified three key pathways that harbored the largest number of up-regulated genes, namely, those involved in metabolism (26 genes), protein processing in the ER (22 genes), and RNA transport (21 genes) (Supporting Information, Table S1). Genes that were up-regulated in the ER protein processing pathway had roles in ubiquitin attachment, protein transport, folding, and synthesis. SEC63, which plays a role in post-translational protein translocation in ER, was up-regulated to the greatest extent by **41** (48× compared to untreated cells).

The gene expression profile of curcumin-treated NB4 cells was also investigated under similar conditions but at a higher concentration (5 μM). Interestingly, the key pathways affected by curcumin were also those identified for **41** (Table S1). In the ER protein processing pathway, 21 common genes were up-regulated to almost the same levels as **41**. SEC63 was also the most highly up-regulated gene in curcumin-treated NB4 cells. Only a handful of genes were down-regulated by **41** (18) and curcumin (12). Of these, six genes were down-regulated by both compounds (Table S1), and they were involved in cell development and proliferation (OCM, RGL2, CFB), protein translation (NXF2, MRPL36), and DNA-binding transcriptional repression (THAP5).[36,37]

To validate the microarray results, we determined the expression of randomly selected genes by real-time PCR. These were UBE2E1, EIF2AK2, SEC62, LMAN1 which were up-regulated by both compounds in the ER protein processing pathway and the DNA-binding transcriptional repressor THAP5 which was down-regulated. Figure 4 shows that **41** and curcumin affected the expression of these genes as predicted from the microarray results. Although the fold-changes induced by **41** and curcumin were broadly comparable (2- to 3-fold), they were elicited at different concentrations (50 nM **41** versus 5 μM curcumin).

2.8. Michael Acceptor Reactivities of Thiopyranone Dioxides 41 and 227. Michael adduct formation has been implicated in the induction of ER stress.[38] Briefly, Michael acceptors react with cysteine residues on secretory proteins and disrupt the normal sequence of disulfide bond formation necessary for protein folding. As the load of misfolded protein increases, ER stress is exacerbated. Thus far, we have reasoned that the thiopyranone dioxides sensitized NB4 cells to ER stress induced apoptosis by promoting levels of misfolded N-CoR. It is conceivable that the Michael acceptor reactivities of the α,β-unsaturated dienone motif in these compounds may intercept the folding process of proteins (other than or including N-CoR). Hence, it was of interest to assess the Michael acceptor reactivities of these compounds. Here, we employed a proton NMR spectroscopic method to monitor the reaction of **41**, **227**, and curcumin with cysteamine, a nucleophile with an affinity for Michael acceptors.[39] Briefly, the spectrum of the test compound in deuterated DMSO was first recorded, after which a 2-fold excess of cysteamine was added and the spectrum recorded again after 5 min. The reaction of curcumin with cysteamine had been reported by this method,[39] and our

Table 2. Concentration of Test Compound (41, Curcumin, Bortezomib) Required To Inhibit Catalytic Activity of Human 26S Proteasomal Subunits by 50% (IC_{50}) after 2 and 4 h, 25°C

	$IC_{50}{}^{a}$ (nM)					
	41		curcumin		bortezomib	
human 26S proteasomal catalytic subunit	2 h	4 h^{b}	2 h	4 h^{b}	2 h	4 h^{b}
trypsin-like	26000 ± 2000	1900 ± 200	40000 ± 4000	2500 ± 200	5.3 ± 0.4	1.9 ± 0.2
caspase-like	26000 ± 0	3800 ± 0	26000 ± 1000	4800 ± 700	6.6 ± 0.7	1.2 ± 0.3
chymotrypsin-like	45000 ± 5000	5400 ± 900	48000 ± 0	3800 ± 800	2.7 ± 0.3	1.0 ± 0.0

^{a}Mean and SD for n = 3 separate determinations. ^{b}Basal activity of catalytic subunits at 4 h was approximately 80% of basal activity levels at 2 h.
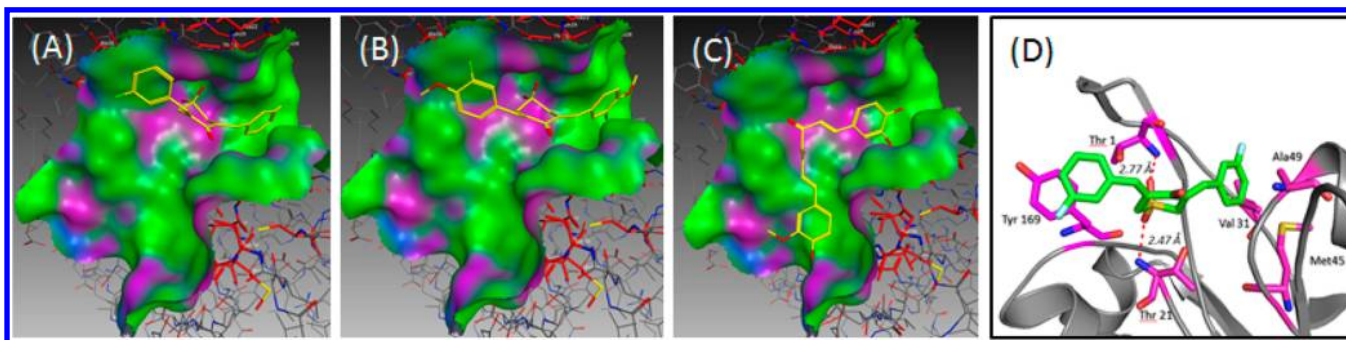
Figure 5. Orientation of (A) **41**, (B) **227**, and (C) curcumin in the binding pocket of β5 subunit of the 20S proteasome (PDB 1IRU).[41] The binding pocket is "T" shaped with lipophilic (green), H bonding (magenta), and mildly polar (blue) areas (MOE, version 11). **41** (A) and **227** (B) were oriented along the horizontal arm of the T, and their phenyl rings established $\pi-\pi$/hydrophobic interactions with the lipophilic residues at the ends of the horizontal arm. These were Tyr 169 on one end and Ala20, Ala49, Val31, Met45 on the other end. (C) Curcumin had an "L-shaped" orientation and occupied part of the horizontal and vertical axes. The vertical arm comprised a limited hydrophobic region at the base of the T. The enolic OH was H-bonded to Thr1 and Ser130, and one of its phenyl rings established nonpolar interactions with the hydrophobic domain (Val128, Ala46, Met97) at the base of the vertical axis. (D) Hydrogen bonding and $\pi-\pi$ and nonpolar interactions of **41** with binding pocket.

findings showed a loss of olefinic protons (Hα, Hβ) and appearance of multiple peaks in the region 6.50−7.50 ppm (due to adduct formation with cysteamine) as reported earlier (Supporting Information, Figure S4).[39] Because of the symmetrical nature of **41** and **219**, the two olefinic protons Hα were observed as a single peak at 7.85 ppm (**41**) and 7.80 ppm (**227**). On addition of cysteamine, the spectra showed significant reduction in peak intensities, changes in chemical shifts, and the appearance of multiple peaks in the region 6.90−8.00 ppm that were indicative of Michael adduct formation (Supporting Information, Figure S4).

2.9. Thiopyranone Dioxides 41, 221, and 227 Inhibit 26S Proteasomal Activity in Vitro. Curcumin was reported to promote accumulation of misfolded N-CoR by blocking its degradation by N-CoR specific proteases and the proteasome.[16] *O*-Sialoglycoprotein endopeptidase (OSGEP), a protease selectively expressed in APL cells to cleave misfolded N-CoR,[12] was inhibited by curcumin but not **41** (data not shown). Thus, **41** may intercept the degradation of misfolded N-CoR by other means, possibly by inhibiting the proteasome. To investigate this possibility, we evaluated **41** for inhibition of purified 26S proteasomal subunits (chymotrypsin-like, trypsin-like, caspase-like). Briefly, the proteasome was incubated with various concentrations of **41** for 2−4 h at 25 °C, after which residual proteasomal activity was evaluated with luminogenic peptide substrates that were specifically cleaved by the different catalytic subunits. **41** was found to inhibit trypsin, caspase, and chymotrypsin-like activities to the same extent, based on IC_{50} values (Table 2). Inhibitory potencies were comparable to curcumin (a known proteasomal inhibitor)[40] but significantly weaker than the positive control bortezomib. We noted that inhibition increased with incubation time and in the case of **41**,

lengthening the incubation time from 2 to 4 h led to a decrease in IC_{50} values from 26−45 μM to 2−5 μM. Less pronounced decreases were observed for bortezomib under similar conditions.

To determine the structural determinants of **41** that could have contributed to proteasomal inhibition, we docked **41** onto the β5 subunit (chymotrypsin-like activity) of the human 20S proteasome (PDB 1IRU).[41] The binding pocket had a skewed "T" shape, with lipophilic residues at both ends of the horizontal arm of the T (Tyr169, Ala20, Ala49, Val31, Met45). Sandwiched between these lipophilic domains was a cluster of H bonding residues (Thr1, Thr21, Ser130, Lys33). Inspection of the top ranked poses of **41** showed that it was aligned along the horizontal arm of the T shaped pocket, with one terminal phenyl ring involved in $\pi-\pi$ stacking with Tyr 169 and the other flanked by nonpolar residues Ala49, Val31, and Met45. The sulfonyl oxygen atoms were engaged in H bonding with Thr1 (N-terminal NH$_2$) and Thr21 (backbone NH) (Figure 5A and Figure 5D). We found similar poses for two other thiopyranone dioxides **221** and **227** (Figure 5B), which suggested that the scaffold was well placed for productive H bonding and $\pi-\pi$ and hydrophobic interactions with the β5 binding pocket. Curcumin was also accommodated in the binding pocket, but unlike **41**, it had an L-shaped pose and occupied the vertical arm and half of the horizontal T arm (Figure 5C).

Next, we assessed **41** for inhibition of the proteasome in NB4 cells. Briefly, **41** was incubated with NB4 cells (48 h, 37 °C), after which residual proteasomal activities were determined with fluorogenic peptide substrates specific to the catalytic subunits. **41** was found to completely inhibit caspase-like, trypsin-like, and chymotrypsin-like activities at 1 μM (Supporting Information, Figure S5) which was not in keeping

with its modest in vitro inhibitory activities (IC$_{50}$ = 2−5 μM) observed earlier. The different experimental conditions employed in these assays may have contributed to the contrasting results, but the possibility of **41** inhibiting other cellular proteases that could hydrolyze the fluorogenic substrates should not be entirely discounted.

3. DISCUSSION

The susceptibility of cross-conjugated β-diketone linker in curcumin to hydrolysis and metabolism has made it a focal point for structural modification aimed at rectifying these shortcomings in curcumin. A review of the literature shows that this moiety is either replaced or altered to give, among others, Knoevanagel conjugates, monocarbonyl cross-conjugated dienones, and cyclized monocarbonyl cross-conjugated dienones.[25] In an earlier investigation, we focused on the APL growth inhibitory activities of several monocarbonyl cross-conjugated dienones (monocarbonyls, cyclopentanones, cyclohexanones, thiopyranones, piperidinones).[27] Briefly, we found superior (submicromolar) activity among the thiopyranones and piperidinones. These were versatile scaffolds that supported fluorinated and oxygenated (OH, OCH$_3$) substituents at the terminal phenyl rings with limited variations in activity. In contrast, there was a noticeable preference for dioxygenated (di-OCH$_3$, OH-OCH$_3$) over fluorinated substituents among monocarbonyls, cyclopentanones, and cyclohexanones. However, activities were capped at low micromolar levels even for the most promising analogues. In this report, we explored the potential of the thiopyranone scaffold by undertaking asymmetrical substitution of phenyl rings, phenyl to pyridine replacement, and thiopyranone to thiopyranone dioxide conversion. The focus on thiopyranone rather than the equipotent piperidinone scaffold was largely prompted by the considerable work reported on the latter and which has resulted in the piperidinone EF24 (**42** in this report), arguably one of the most widely investigated and promising curcumin analogue identified to date.[29,30,42] Of the modifications carried out, oxidation to give thiopyranone dioxides was the most promising, yielding compounds (**40**, **41**, **221**, **224**, **227**) with nanomolar potencies on the APL cell line NB4. In comparison, the phenyl to pyridine replacement showed only incremental improvements in activity when compared to the original thiopyranone leads **32**, **34**, and **212**. Asymmetric substitution of the terminal phenyl rings of thiopyranone proved disappointing in that growth inhibitory activity was either no better or even weaker than the original leads. Several instances of scaffold-dependent differences in the structure–activity relationship were noted. For example, thiopyranones showed a regioisomeric preference for 2- and 3-pyridinyl terminal rings that was noticeably absent among previously synthesized cyclohexanones bearing the same phenyl to pyridine replacement. A comparison of growth inhibitory IC$_{50\ NB4}$ values showed that the thiopyranone dioxide analogue consistently outperformed its cyclohexanone, thiopyranone, and piperidinone counterparts. Notably, thiopyranone dioxide **40** (IC$_{50\ NB4}$ = 80 nM) was at least 3 times more potent than piperidinone **42**/EF24 (IC$_{50}$ = 0.29 μM). Taken together, the impressive activities of the thiopyranone dioxides were clear advantages not observed with the earlier compounds[27] or other scaffolds investigated in this report.

When evaluated for time-dependent hydrolytic degradation, the thiopyranone dioxides **41** and **227** were comparable to thiopyranone **219** but more stable than curcumin at 48 and 72 h time points. Notably, nearly 30−40% of thiopyranone dioxides **41** and **227** were detected after 72 h compared to less than 10% for curcumin. Other scaffolds were not investigated but based on an earlier report;[34] the nature of the connecting linker and substitution on the terminal aryl rings strongly influenced hydrolytic stability. Thus, the modest stabilities of thiopyranone dioxides could conceivably be improved by appropriate modifications at the terminal aryl rings.

There is growing interest in the pharmacological targeting of ER stress signaling pathways in cancer.[11,17] The ideal agent should paradoxically aggravate pre-existing stress levels in tumor cells to the point that prosurvival mechanisms are overwhelmed and overtaken by the prodeath arm of the UPR. Curcumin, by inhibiting the degradation of misfolded N-CoR, sensitized APL cells to ER stress-induced apoptosis.[16] A monocarbonyl dienone analogue of curcumin [1E,4E-1,5-bis(2,3-dimethoxyphenyl)penta-1,4-dien-3-one] acted in a mechanistically related manner on human lung cancer H460 cells.[43] Thus, we rationalized that the potent growth inhibitory activities of the thiopyranone dioxides on NB4 cells could likewise be linked to the induction of ER-stress induced apoptosis. To that end, we have shown that the thiopyranone dioxide **41** induced build-up of misfolded N-CoR in the cytosol of NB4 cells. Elevated levels of chaperone proteins (PDI, GRP73, HSP60) and ER stress sensors (PERK, IRE1, and constituent proteins) implicated heightened levels of ER stress in NB4 cells treated with **41**. Notably, the proteins in the PERK and IRE1 signaling arms of the UPR remained elevated for up to 48 h, pointing to sustained stress levels in the cells. Furthermore, increases in GADD34 and ASK1, which are critical to the commitment phase of ER stress-induced apoptosis, signaled a transition of the UPR from a prosurvival to a prodeath mode. Microarray analysis of over 28 000 genes in NB4 cells confirmed that **41** preferentially up-regulated protein processing genes that were relevant to the activation of the UPR. Taken together, there is corroboratory evidence pointing to a consequential role for the UPR in the induction of apoptosis by **41** in NB4 cells.

However, the question remains as to the incipient events that could have triggered the accumulation of misfolded proteins and the cascade of prodeath reactions described earlier. We have shown that **41**, **219**, and **227** were Michael acceptors. Their reactivities could conceivably interfere with the normal course of protein folding and hence exacerbate ER stress. Another possibility is the inhibition of the proteasome which by curtailing the degradation of misfolded proteins would compound ER stress with expected consequences. We showed that **41** inhibited purified 26S proteasome at low micromolar concentrations and molecular docking indicated that it was well placed for productive H bonding and $\pi-\pi$ and hydrophobic interactions to the β5 chymotrypsin binding pocket. However, the discrepancy between the cell based and in vitro proteasomal inhibitory potencies of **41** indicated the need for more robust evidence to support proteasomal involvement in intercepting the degradation of misfolded proteins. Notwithstanding these mechanistic aspects, the thiopyranone dioxide scaffold is distinguished from other monocarbonyl dienone analogues of curcumin by the potent growth inhibitory activities of several members on malignant APL cells.

4. EXPERIMENTAL SECTION

4.1. General Details for Chemical Syntheses. Reagents (synthetic grade or better) were obtained from commercial suppliers (Sigma-Aldrich Chemical Co. Inc., Singapore; Alfa Aesar, MA, USA)

and used without further purification. ^{1}H and ^{13}C NMR spectra were recorded on a Bruker ACF (DPX 400 MHz). Chemical shifts are reported in parts per million (ppm). The residual solvent peak was used as an internal reference. Analytical thin layer chromatography (TLC) was performed with Merck precoated TLC plates, silica gel 60F-254, layer thickness of 0.25 mm. Flash chromatography separations were performed on Merck 60 (0.040−0.063 mm) mesh silica gel. Nominal mass spectra were analyzed on LcQ Finnigan MAT mass spectrometer with chemical ionization (APCI) as probe. High resolution accurate mass spectra were analyzed on Bruker micrOTOF-QII mass spectrometer with chemical ionization (APCI) as probe. Spectroscopic data and reaction yield of final compounds are given in Supporting Information. Purity of final compounds was verified by combustion analysis (PerkinElmer PRE-2400 elemental analyzer) or by reverse phase HPLC on two different solvent systems (isocratic mode). Details are given in Supporting Information. Unless otherwise stated, combustion analyses for C and H fell within 0.4% of theoretical values, and compounds analyzed on HPLC were found to be of ≥95% purity on both solvent systems.

4.2. General Procedure for Syntheses of 201, 206, 207−214, 228, 229 by Aldol Condensation under Basic Conditions. A solution of the reacting ketone (cyclohexanone, tetrahydrothiopyran-4-one or piperidin-4-one) (1 mmol) in 0.3% (w/v) NaOH in aqueous ethanol (50% v/v, 6 mL) was stirred at room temperature (25 °C) in a round-bottom flask sealed with a rubber septum. A solution of the substituted benzaldehyde (2.1 mmol) in ethanol (1 mL) was added dropwise to the stirred solution over 5 min, after which stirring was continued overnight at room temperature. The precipitated solids were removed by vacuum filtration, washed with cold ethanol, and dried under vacuum. In most cases, the product was purified by column chromatography with hexane/ethyl acetate as eluting solvents. For **228** and **229**, the free base was dissolved in ethyl acetate and acidified with 6 M HCl to afford the corresponding HCl salt which was removed by filtration under reduced pressure and washed with ethyl acetate.

4.3. General Procedure for Syntheses of 215, 216, 230, 231 by Aldol Condensation under Acidic Conditions. A solution of the reacting ketone (tetrahydrothiopyran-4-one or piperidin-4-one) (0.5 mmol) in denatured ethanol (2 mL) was stirred at room temperature (25 °C) in a round-bottom flask sealed with a rubber septum. Then 6 M HCl (25 μL) was added followed by the substituted benzaldehyde (1 mmol). The mixture was heated to 30−60 °C on an oil bath, and the progress of the reaction was periodically monitored by TLC over 18−24 h. Solids were removed by vacuum filtration and washed with ethanol. In most cases, the product was purified by column chromatography with hexane/ethyl acetate as eluting solvents followed by recrystallization in suitable solvents.

4.4. General Procedure for Syntheses of 40, 41, 221−227. The corresponding 3,5-bis(substituted benzylidene)-tetrahydrothiopyran-4-one required for the syntheses of **40**, **41**, **221**, **222**, and **226** were synthesized as reported.[23] The 3,5-bis(substituted benzylidene)tetrahydrothiopyran-4-ones **211**, **213−215** were the starting materials for **223−225**, **227**. In a dry round-bottom flask was added the 3,5-bis(substituted benzylidene)tetrahydrothiopyran-4-one (0.5 mmol) in glacial acetic acid (3.5 mL) which was then stirred at 30−40 °C, followed by addition of 30% hydrogen peroxide (320 μL), The mixture was stirred at 60 °C for 6−24 h during which time the reaction mixture was periodically monitored by TLC. The flask was cooled to room temperature, distilled water was added, and the mixture was cooled further in ice to induce the precipitation of the product as a yellow solid. It was removed by filtration, washed with distilled water, purified by column chromatography with hexane/ethyl acetate as eluting solvents, and recrystallized in suitable solvents.

4.5. 2-(3-Fluorobenzylidene)cyclohexanone (1). A solution of cyclohexanone (4 mmol) in ethanol (4 mL) was stirred at 65 °C. 3-Fluorobenzaldehyde (1 mmol) in ethanol (1 mL) was added dropwise to the stirred solution over 5 min, followed by 6 M HCl (10 μL). Stirring was stopped when the starting benzaldehyde was not detected by TLC. The mixture was evaporated under reduced pressure and the residue was dissolved in dichloromethane and extracted with brine.

The organic layer was removed in vacuo, and the residue was purified by column chromatography with hexane/ethyl acetate as eluting solvents.

4.6. (3-[(3-Fluorobenzylidene)dihydro-2H-thiopyran-4(3H)-one) (2). To a clear and dry three-necked round-bottom flask was added lithium diisopropylamide (LDA) in tetrahydrofuran (THF) (2 M, 4 mmol). The mixture was cooled to −78 °C in a dry ice and acetone slurry, and the flask was purged with argon for 3−5 min. Tetrahydrothiopyran-4-one (2.0 mmol) was dissolved in anhydrous THF (1 mL) and added dropwise to the stirred LDA mixture at −78 °C over an argon atmosphere. After 1 h, 3-fluorobenzaldehyde (2 mmol) in anhydrous THF (1 mL) was added dropwise to the mixture over 10 min. The progress of the reaction was periodically monitored by TLC over 6 h. THF was removed in vacuo followed by extraction with brine/dichloromethane to give a yellow oil which was dissolved in toluene (3 mL). *p*-Toluenesulfonic acid (0.1 mmol) was added, and the mixture was stirred at 90 °C over 1.5 h. The mixture was evaporated under reduced pressure and worked up with dichloromethane and brine to give the crude product which was purified by column chromatography with hexane/ethyl acetate as eluting solvents.

4.7. General Procedure for Syntheses of 202−205, 217−220. The procedure described in section 4.3 was followed with minor changes. A solution of the ketone **1** or **2** (0.5 mmol) in denatured ethanol (2 mL) was stirred at room temperature (25 °C) in a round-bottom flask sealed with a rubber septum. Then 6 M HCl (25 μL) was added followed by the substituted benzaldehyde (0.5 mmol). The mixture was heated to 65 °C on an oil bath, and the progress of the reaction was periodically monitored by TLC over 1−2 days. The mixture was evaporated under reduced pressure and worked up with dichloromethane and brine to give the crude product which was purified by column chromatography with hexane/ethyl acetate as eluting solvents.

4.8. Hydrolytic Stability. The method described by Liang et al.[34] was followed with some modifications. Test compound (1 mg) was dissolved in 0.5 mL of PBS (1×, pH 7.4) comprising DMSO (50%) and sodium carboxymethylcellulose (0.3%) and kept in the dark at 25 °C. Aliquots were withdrawn at the stated time period (0, 24, 48, 75 h), diluted 100× with methanol, and analyzed by HPLC on a Shimadzu SPD-20A HPLC system. Samples were separated on a Poroshell 120 EC-C18 column (Agilent Technologies) at 80% methanol, 20% H_2O; flow rate of 0.6 mL/min. The % degradation was assessed from a comparison of peak areas of signals attributed to test compound at the start of experiment and after $x = 24$, 48, and 75 h.

$$\% \text{ degradation} = \frac{(\text{peak area at } 0\,\text{h}) - (\text{peak area at } x\,\text{h})}{\text{peak area at } 0\,\text{h}} \times 100$$

The determinations were made on two freshly prepared solutions of test compound. Results were analyzed for statistical significance using one-way ANOVA with post-Bonferroni multiple comparison test (GraphPad Prism, version 3.0).

4.9. NMR Spectroscopic Assay. The method described by Avonto et al.[39] was followed with some modifications. Test compound (4 mg) was dissolved in 0.5 mL of DMSO-d_6, and the ^{1}H NMR spectrum was recorded immediately on a 400 MHz Bruker ACF NMR instrument. Cysteamine (6 mg) was added, and the mixture was vortexed for 5 min after which the ^{1}H NMR spectrum was recorded. The residual solvent peak was used as an internal reference. NMR spectra were analyzed using MestRec Research Software (Bajo, Spain).

4.10. Cell Lines and Reagents. The *all-trans*-retinoic acid sensitive acute promyelocytic leukemia cell line NB4 and its resistant variant NB4-R1 were generous gifts from Dr. Y. Homma (Department of Biosignal Research, Tokyo Metropolitan Institute of Gerontology, Japan) and Dr. M. Lanotte (INSERM U-301, Centre G. Hayem, Hôpotal Saint-Louis, France), respectively. Leukemic cell lines were maintained in Rosewell Park Memorial Institute 1640 (RPMI, Gibco) medium, IMR90 in Eagle's minimum essential medium (EMEM, Sigma-Aldrich), and MCF10A in Dulbecco's modified Eagle medium (DMEM, Gibco) containing penicillin/streptomycin (50 U/10 μg/mL) and heat-inactivated fetal bovine serum (10%) at 37 °C in a humidified

5% CO_2 atmosphere. They were used within 10 passages for biological assays. Buffers and reagents were obtained from Invitrogen Life Technologies (CA, USA) unless otherwise stated. Curcumin was purchased from Sigma-Aldrich (Singapore) and dissolved in DMSO. CellTiter 96 AQueous One solution assay was obtained from Promega (Madison WI). 7-Amino-4-methylcoumarin (AMC) conjugated fluorogenic peptide substrates Boc-Leu-Arg-Arg-AMC, Suc-Leu-Leu-Val-Tyr-AMC, Z-Leu-Leu-Glu-AMC (for the proteasomal trypsin-like, chymotrypsin-like, and peptidylglutamyl peptide hydrolyzing (PGPH or caspase)-like activities, respectively) were purchased from Biomol, Enzo Life Sciences Inc. (Farmingdale, NY). The in vitro activity of human 26S proteasome (Biomol, Enzo Life Sciences, Farmingdale, NY) was evaluated on the Proteasome Glo Assay System (Promega, Madison, WI).

Primary antibodies anti-ASK1 (rabbit, 1:1000), anti-caspase 3 (rabbit, 1:1000), anticleaved caspase 3 (rabbit, 1:1000), anti-eIF2α (rabbit, 1:1000), anti-PARP (rabbit, 1:1000), anti-phospho ASK1 (rabbit, 1:2000), anti-phospho eIF2α (rabbit, 1:1000), anti-phospho SAPK/JNK (mouse, 1:1000), anti-SAPK/JNK (mouse, 1:1000) were purchased from Cell Signaling. Antibody anti-β-actin (mouse, 1:10000) was purchased from Sigma. Antibodies anti-N-CoR C-20 (goat, 1:500), anti-GADD34 (rabbit, 1:1000), anti-GRP78 (goat, 1:2000), anti-HSP60 (rabbit, 1:5000), anti-PERK (rabbit, 1:2000), anti-phosphoPERK (rabbit, 1:2000) were purchased from Santa Cruz Biotechnology. Secondary horseradish peroxidase antibodies including goat anti-mouse, goat anti-rabbit, mouse-antigoat (1:10 000) were purchased from Zymed Laboratories.

4.11. Cell Viability Assay. Effect of test compounds on viability of cells (NB4, NB4-R1) were determined by the MTS [3-(4,5-dimethylthiazol-2-yl)-5-(3-carboxymethoxyphenyl)-2-(4-sulfophenyl)-2H-tetrazolium] assay. Leukemic cells were seeded at 3500 cells per well, respectively. Stock solutions of test compounds were prepared in DMSO and diluted with respective media to give a final concentration of 0.5% v/v DMSO. Cells were treated with at least six concentrations of test compound for 72 h at 37 °C in a humidified 5% CO_2 atmosphere. Concentrations investigated span the dynamic range of the inverted S-shaped cell viability curve. After this time, 10 μL of MTS (CellTiter 96 AQueous One solution assay) was added to each well under dim light. The plates were incubated in the dark at 37 °C for 4 h, after which absorbance readings were taken at 490 nm on a microplate reader (Biorad Ultramark microplate imaging system). Cell viability was determined from the expression

$$\text{cell viability (\%)} = \frac{A - C}{U - Z} \times 100$$

where A is the absorbance of wells containing cells and test compound, C is the absorbance of test compound at 490 nm, U is the absorbance of untreated cells in medium and 0.5% DMSO, and Z is the absorbance of medium and 0.5% DMSO. The IC_{50} of test compound (concentration required to reduce cell viability to 50% of control values from untreated cells) was determined using GraphPad Prism (version 3.0, GraphPad software, San Diego, CA). Each concentration of test compound was evaluated in triplicate for each run, and the assay was carried out on at least three separate occasions using at least two freshly prepared stock solutions.

4.12. Apoptosis Determination Using Flow Cytometry. The annexin V-FITC apoptosis detection kit (Sigma-Aldrich, APOAF) was used. NB4 cells were seeded at 10^5 cells/mL and treated with compounds at respective concentrations (final 0.1% DMSO). After incubation at 37 °C in a humidified 5% CO_2 atmosphere for 48 h, the cells were transferred to a 50 mL Falcon tube, pelleted by centrifugation (200g, 5 min), and washed twice with ice-cold 1× PBS. The cell pellet was declumped thoroughly and resuspended in 1× binding buffer at density of 10^6 cells/mL. Annexin V-FITC conjugate protein (5 μL) and propidium iodide solution (1 μL) were added to cell suspension (500 μL) and incubated at room temperature for 10 min in the dark. Flow cytometric analysis was carried out on the Cytomation Cyan LX instrument (Dako, Fort Collins, Co, USA) using the Summit software. Unstained treated cells and treated cells single-stained with annexin V-FITC or propidium iodide only were used for

calibration and compensation. 20 000 cells were read for each sample determination. Each compound was evaluated in at least three independent experiments using two or more freshly prepared stock solutions of test compound.

4.13. Western Blotting. The detection of N-CoR by Western blotting was carried out as described in an earlier report.[27] For the other proteins, the following method was followed. Treated NB4 cells were harvested as described in section 4.11 except that cell lysis buffer (Sigma-Aldrich C2978) containing cOmplete protease inhibitor (1×, Roche) was added. Crude lysates (1 μg/mL) were stored at −80 °C. Protein samples were separated on SDS−PAGE using 8%, 10%, or 12% resolving gel and gradient voltage of 80 V for the first 30 min followed by a gradual increase to 100 V over 30 min and then fixed at 100 V for the remaining time. Separated protein samples were transferred onto prewetted PVDF membrane using a wet trans-electroblotting system (Bio-Rad Inc., England) at a constant current of 80 V (120 min, 4 °C) using transfer buffer. Methanol (10% v/v) was added to the transfer buffer prior to use. The membrane was blocked with 5% milk or BSA in PBS or TBS containing 0.1% v/v Tween 20 (PBS-T or TBS-T) for 1 h, 25 °C followed by incubation (overnight, 4 °C) with the respective primary antibodies in 5% milk or BSA in PBS-T or TBS-T with slow shaking. The membrane was washed with PBS-T or TBS-T (3×, 10 min per wash) and incubated with horseradish peroxidase-conjugated secondary antibody in 5% milk or BSA in PBS-T or TBS-T (1 h, 25 °C). The unbound secondary antibodies were removed by washing with PBS-T or TBS-T (3×, 10 min per wash). The immunoreactive bands were detected by Western Lightning Chemiluminescence Reagent Plus (PerkinElmer) using a Konica Minolta SRX-101A film processor.

4.14. Immunostaining and Fluorescence Microscopy for Detection of N-CoR in Nuclear and Cytosolic Compartments in NB4 Cells. A previously reported method was followed.[27]

4.15. Microarray Chip Hybridization and Pathway Analysis. Total RNA was isolated from treated cells using the RNeasy Plus Mini kit (Qiagen GmBH, Hilden, Germany) following the manufacturer's protocol. mRNA concentrations were measured using the Nanodrop 1000 (Thermo Scientific), and samples with OD_{260nm}/OD_{280nm} between 1.9 and 2.1 were subjected to electrophoresis on a 1% agarose gel. The gel was stained with ethidium bromide to determine the presence of 25S and 16S rRNA. Samples were submitted to Affymetrix Origin Laboratories (Singapore) for a total RNA quality check using the Agilent bioanalyzer, after which the samples were hybridized onto Affymetrix human gene 1.0 ST arrays. Data processing was carried out by Sciencewerke Pte Ltd. (Singapore) and involved calibrating the background level and normalizing/transforming the intensities of the probes. Briefly, the bioconductor package Limma was used to assess differential expression between control and treated samples. The Benjamini & Hochberg multiple testing adjustment method was applied to the p-values, and genes with adjusted p-values of <0.05 were used for further gene expression comparison between **41** and curcumin. The KEGG pathway database was used to analyze the profiles of these genes.

4.16. Validation by Real-Time PCR. RNase-free water was added to 2 μg of RNA and 3 pmol of oligo-dT (18-mer) to give a final volume of 21 μL. The mixture was incubated at 65 °C, 15 min and immediately quenched on ice thereafter. A mastermix of 10 μL of 5× RT buffer, 1 μL of 25 mM dNTPs, 0.5 μL of RNasin inhibitor, 1 μL of murine reverse transcriptase and sterile water was prepared to a total volume of 29 μL for each sample. The mastermix was added to the RNA and mixed. The sample was incubated at 42 °C, 1 h for the generation of cDNA. PCR amplification was carried out in 50 μL volumes containing 1 μL of 10× template, 1× PCR reaction buffer, 200 nM each dNTP, 0.8 μM each primer, and 1.5 units of DNA polymerase. Real-time PCR of selected genes was carried out using the TaqMan gene expression assay system (Applied Biosystems, CA, USA) and recorded using the ABI 7500 fast PCR system (Applied Biosystems, CA, USA). The qRT -PCR reaction conditions and list of TaqMan primers are given in Supporting Information, Tables S2 and S3.

4.17. In Vitro Activity of Human 26S Proteasome. The activity of human 26S proteasome was evaluated using proteasome Glo

3-substrate system following the manufacturer's instructions. The kit comprised luminogenic substrates for chymotrypsin-like (Suc-LLVY-aminoluciferin), trypsin-like (Z-LRR-aminoluciferin), and caspase-like (Z-nLPnLD-aminoluciferin) activities. Substrate cleavage liberates aminoluciferin, which in the presence of luciferase is oxidized to oxyluciferin with emission of light. The enzyme (1 μg/mL) was incubated with test compound (**41**, curcumin, or bortezomib) for 2 or 4 h at 25 °C, after which the substrate-containing proteasomal Glo reagent was added and luminescence measured after 30 min. Readings in the presence of test compound were corrected for background luminescence (blank) and expressed as a % of control luminescence (absence of test compound) for the determination of IC_{50}. Determinations were repeated thrice.

4.18. Inhibition of 26S Proteasome Activity in NB4 Cells. The proteasomal inhibition assay described earlier[27] was followed with some modifications. NB4 cells were seeded at 10^5 cells/mL and treated with a known concentration of test compound (final concentration of DMSO, 0.1%). After incubation at 37 °C in a humidified 5% CO_2 atmosphere for 48 h, the cells were transferred to a 50 mL Falcon tube, pelleted by centrifuging (200g, 5 min), and washed twice with ice-cold 1× PBS. The cells were then transferred to a microcentrifuge tube and 4 times the cell pellet volume of cell lysis buffer (Sigma-Aldrich C2978) was added. The cells were subjected to gentle homogenization using a 27G needle and syringe and allowed to stand over ice with frequent agitation for 30 min. The lysates were centrifuged at 10 000 rpm, 5 min, 4 °C. Protein concentration in the supernatant was determined and normalized using BCA protein assay kit (Pierce Laboratories, IL, USA). Proteasomal activity was determined immediately using 2 μg (10 μL) of total protein per well. Substrates that were specific for each catalytic site of the proteasome were Boc-Leu-Arg-Arg-AMC (60 μM) for trypsin-like, Suc-Leu-Leu-Val-Tyr-AMC (50 μM) for chymotrypsin-like, and Z-Leu-Leu-Glu-AMC (30 μM) for caspase-like activity. Concentrations of peptide substrates were chosen based on the K_m (Supporting Information, Figure S6) of the catalytic unit. K_m measurement was carried out by measuring the rate of reaction at each substrate concentration (4−200 μM) with 2 μg (10 μL) of protein lysate. K_m and V_{max} of each substrate were calculated with the Michaelis−Menten equation. Reactions were initiated by substrate addition (90 μL). The release of the fluorescent tag AMC on hydrolysis of substrate was monitored for 1 h at λ_{ex} = 360 nm and λ_{em} = 460 nm (25 °C) on an Infinite 200 microplate reader (Tecan). Representative plots are shown in Figure S7 (Supporting Information). Inhibition of proteasomal activity was determined from the reaction velocities (gradients) of treated and untreated (control) cell lysates.

$$\% \text{ inhibition} = \frac{\text{gradient}_{control} - \text{gradient}_{treated}}{\text{gradient}_{control}} \times 100$$

The assay was carried out on at least three separate occasions using two (or more) freshly prepared stock solutions of test compound.

4.19. Molecular Docking. Human 20S proteasome was retrieved from the RCSB Protein Data Bank (PDB 1IRU).[41] The β5 chymotrypsin catalytic subunit was identified and processed for docking using LigX in the software Molecular Operating Environment (MOE, version 2011, Chemical Computing Group, Montreal, Canada). Test molecules (**41**, **206**, **211**, **219**, **220**, **221**, **227**, curcumin) were also prepared on MOE. Docking simulation was carried out on GOLD, version 5.2 (Cambridge Crystallographic Data Centre Software Ltd., Cambridge, U.K.) with default GA settings. The binding pocket was defined by the atoms within 10 Å radius of the Thr1 hydroxyl oxygen atom. GOLD uses a genetic algorithm (GA) for docking flexible ligands into the binding pocket to explore the full range of ligand conformational flexibility.[44] The GOLD score was used to select the best docked conformations of test compounds in the binding pocket.

ASSOCIATED CONTENT

Ⓢ Supporting Information
Spectroscopic data of synthesized compounds; evaluation of compound purity by reverse phase HPLC; time dependent hydrolytic stabilities of curcumin, **41**, **219**, and **227** in phosphate buffer; induction of apoptosis in NB4 cells by **41**, **219**, and **227**; compounds **41**, **219**, and **227** induced ER stress and activated UPR-induced apoptosis in NB4 cells; reaction of curcumin, **41**, and **227** with cysteamine; dose-dependent inhibition of the trypsin-like, caspase-like, and chymotrypsin-like activities of the proteasome by curcumin and 41; determination of K_m and V_{max} of substrates used for determination of catalytic activities of NB4 cells; inhibition of trypsin-like, chymotrypsin-like, and caspase-like activities in NB4 cells by curcumin and **41** at a fixed concentration of 1 μM; biological pathways in NB4 cells significantly affected by **41** (50 nM) and curcumin (5 μM), based on KEGG pathway database analysis; list of genes in the ER protein processing pathway that were significantly up-regulated by **41** and curcumin; list of genes that were significantly down-regulated by both **41** and curcumin; real-time PCR reaction reagents and conditions; list of TaqMan primers for real-time PCR. This material is available free of charge via the Internet at http://pubs.acs.org.

AUTHOR INFORMATION

Corresponding Author
*E-mail: phagoml@nus.edu.sg. Phone: 65-65162654.
Notes
The authors declare no competing financial interest.

ACKNOWLEDGMENTS

ABBREVIATIONS USED

ASK1, apoptosis signal regulating kinase 1; ATF, activating transcription factor 6; APL, acute promyelocytic leukemia; elF2α, eukaryotic initiation factor 2; ER, endothelium reticulum; ERAD, endothelium reticulum associated degradation; FACS, fluorescence-activated cell sorting; GADD34, growth arrest and DNA damage inducible protein 34; GRP78, glucose-regulated protein 78; HSP60, heat shock protein 60; IκBα, inhibitor of κBα; IKK, inhibitor of κB kinase; IRE1, inositol-requiring enzyme 1; JNK, c-Jun N-terminal kinase; KEGG, Kyoto Encyclopedia of Genes and Genomes; N-CoR, nuclear co-repressor; NF-κB, nuclear factor κB; OSGEP, O-sialoglycoprotein endopeptidase; PARP, poly (ADP-ribose) polymerase; PCR, polymerase chain reaction; PDI, protein disulfide isomerase; PERK, protein kinase RNA-like endothelium reticulum kinase; PML, promyelocytic leukemia; RARα, retinoic acid receptor α; TNFα, tumor necrotic factor α; UPR, unfolded protein response

REFERENCES

(1) Kakizuka, A.; Miller, W. H., Jr.; Umesono, K.; Warrell, R. P., Jr.; Frankel, S. R.; Murty, V. V.; Dmitrovsky, E.; Evans, R. M. Chromosomal translocation t(15;17) in human acute promyelocytic leukemia fuses RAR alpha with a novel putative transcription factor, PML. *Cell* **1991**, *66*, 663−674.
(2) de The, H.; Lavau, C.; Marchio, A.; Chomienne, C.; Degos, L.; Dejean, A. The PML-RARa fusion mRNA generated by the t(15;17)

translocation in acute promyelocytic leukemia encodes a functionally altered RAR. *Cell* **1991**, *66*, 675−684.

(3) Horlein, A. J.; Naar, A. M.; Heinzel, T.; Torchia, J.; Gloss, B.; Kurokawa, R.; Ryan, A.; Kamei, Y.; Soderstrom, M.; Glass, C. K.; Rosenfeld, M. G. Ligand-independent repression by the thyroid hormone receptor mediated by a nuclear receptor co-repressor. *Nature* **1995**, *377*, 397−404.

(4) Heinzel, T.; Lavinsky, R. M.; Mullen, T. M.; Soderstrom, M.; Laherty, C. D.; Torchia, J.; Yang, W.-M.; Brard, G.; Ngo, S. D.; Davie, J. R.; Seto, E.; Eisenman, R. N.; Rose, D. W.; Glass, C. K.; Rosenfeld, M. G. A complex containing N-CoR, mSin3 and histone deacetylase mediates transcriptional repression. *Nature* **1997**, *387*, 43−48.

(5) Laherty, C. D.; Yang, W.-M.; Sun, J. M.; Davie, J. R.; Seto, E.; Eisenman, R. N. Histone deacetylases associated with the mSin3 Co-repressor mediate mad transcriptional repression. *Cell* **1997**, *89*, 349−356.

(6) Karagianni, P.; Wong, J. HDAC3: taking the SMRT-N-CoRrect road to repression. *Oncogene* **2007**, *26*, 5439−5449.

(7) Lin, R. J.; Nagy, L.; Inoue, S.; Shao, W.; Miller, W. H., Jr.; Evans, R. M. Role of the histone deacetylase complex in acute promyelocytic leukaemia. *Nature* **1998**, *391*, 811−814.

(8) Grignani, F.; De Matteis, S.; Nervi, C.; Tomassoni, L.; Gelmetti, V.; Cioce, M.; Fanelli, M.; Ruthardt, M.; Ferrara, F. F.; Zamir, I.; Seiser, C.; Lazar, M. A.; Minucci, S.; Pelicci, P. G. Fusion proteins of the retinoic acid receptor-alpha recruit histone deacetylase in promyelocytic leukaemia. *Nature* **1998**, *391*, 815−818.

(9) Khan, M. M.; Nomura, T.; Chiba, T.; Tanaka, K.; Yoshida, H.; Mori, K.; Ishii, S. The fusion oncoprotein PML-RAR induces endoplasmic reticulum (ER)-associated degradation of N-CoR and ER stress. *J. Biol. Chem.* **2004**, *279*, 11814−11824.

(10) Verfaillie, T.; Garg, A. D.; Agostinis, P. Targeting ER stress induced apoptosis and inflammation in cancer. *Cancer Lett.* **2010**, *332*, 249−264.

(11) Schonthal, A. H. Pharmacological targeting of endoplasmic reticulum stress signaling in cancer. *Biochem. Pharmacol.* **2013**, *85*, 653−666.

(12) Ng, A. P. P.; Howe Fong, J.; Sijin Nin, D.; Hirpara, J. L.; Asou, N.; Chen, C. S.; Pervaiz, S.; Khan, M. Cleavage of misfolded nuclear receptor corepressor confers resistance to unfolded protein response-induced apoptosis. *Cancer Res.* **2006**, *66*, 9903−9912.

(13) Lane, A. A.; Ley, T. J. Neutrophil elastase cleaves PML-RARalpha and is important for the development of acute promyelocytic leukemia in mice. *Cell* **2003**, *115*, 305−318.

(14) Lane, A. A.; Ley, T. J. Neutrophil elastase is important for PML-retinoic acid receptor activities in early myeloid cells. *Mol. Cell. Biol.* **2004**, *25*, 23−33.

(15) Szegezdi, E.; Logue, S. E.; Gorman, A. M.; Samali, A. Mediators of endoplasmic reticulum stress-induced apoptosis. *EMBO Rep.* **2006**, *7*, 880−885.

(16) Ng, A. P. P.; Chng, W. J.; Khan, M. Curcumin sensitizes acute promyelocytic leukemia cells to unfolded protein response-induced apoptosis by blocking the loss of misfolded N-CoR protein. *Mol. Cancer Res.* **2011**, *9*, 1−11.

(17) Luo, B.; Lee, A. S. The critical roles of endoplasmic reticulum chaperones and unfolded protein response in tumorigenesis and anticancer therapies. *Oncogene* **2013**, *32*, 805−818.

(18) Pae, H. O.; Jeong, S. O.; Jeong, G. S.; Kim, K. M.; Kim, H. S.; Kim, S. A.; Kim, Y. C.; Kang, S. D.; Kim, B. N.; Chung, H. T. Curcumin induces pro-apoptotic endoplasmic reticulum stress in human leukemia HL-60 cells. *Biochem. Biophys. Res. Commun.* **2007**, *353*, 1040−1045.

(19) Ip, S. W.; Wu, S. Y.; Yu, C. C.; Kuo, C. L.; Yu, C. S.; Yang, J. S.; Lin, Z. P.; Chiou, S. M.; Chung, H. K.; Ho, H. C.; Chung, J. G. Induction of apoptotic death by curcumin in human tongue squamous cell carcinoma SCC-4 cells is mediated through endoplasmic reticulum stress and mitochondrial-dependent pathways. *Cell Biochem. Funct.* **2011**, *29*, 641−650.

(20) Wang, L.; Wang, L.; Song, R.; Shen, Y.; Sun, Y.; Gu, Y.; Shu, Y.; Xu, Q. Targeting sarcoplasmic/endoplasmic reticulum Ca(2)+-ATPase

2 by curcumin induces ER stress-associated apoptosis for treating human liposarcoma. *Mol. Cancer Ther.* **2011**, *10*, 461−471.

(21) Wu, S. H.; Hang, L. W.; Yang, J. S.; Chen, H. Y.; Lin, H. Y.; Chiang, J. H.; Lu, C. C.; Yang, J. L.; Lai, T. Y.; Ko, Y. C.; Chung, J. G. Curcumin induces apoptosis in human non-small cell lung cancer NCI-H460 cells through ER stress and caspase cascade- and mitochondria-dependent pathways. *Anticancer Res.* **2010**, *30*, 2125−2133.

(22) Anand, P.; Kunnumakkara, A. B.; Newman, R. A.; Aggarwal, B. B. Bioavailability of curcumin: problems and promises. *Mol. Pharmaceuticals* **2007**, *4*, 807−818.

(23) Sharma, R. A. Phase I clinical trial of oral curcumin: biomarkers of systemic activity and compliance. *Clin. Cancer Res.* **2004**, *10*, 6847−6854.

(24) Yallapu, M. M.; Jaggi, M.; Chauhan, S. C. Curcumin nanoformulations: a future nanomedicine for cancer. *Drug Discovery Today* **2012**, *17*, 71−80.

(25) Esatbeyoglu, T.; Huebbe, P.; Ernst, I. M.; Chin, D.; Wagner, A. E.; Rimbach, G. Curcumin—from molecule to biological function. *Angew. Chem., Int. Ed.* **2012**, *51*, 5308−32.

(26) Agrawal, D. K.; Mishra, P. K. Curcumin and its analogues: potential anticancer agents. *Med. Res. Rev.* **2010**, *30*, 818−860.

(27) Tan, K.-L.; Koh, S.-B.; Ee, R. P.-L.; Khan, M.; Go, M.-L. Curcumin analogues with potent and selective anti-proliferative activity on acute promyelocytic leukemia: involvement of accumulated misfolded nuclear receptor co-repressor (N-CoR) protein as a basis for selective activity. *ChemMedChem.* **2012**, *7*, 1567−1579.

(28) Brown, A.; Shi, Q.; Moore, T. W.; Yoon, Y.; Prussia, A.; Maddox, C.; Liotta, D. C.; Shim, H.; Snyder, J. P. Monocarbonyl curcumin analogues: heterocyclic pleiotropic kinase inhibitors that mediate anticancer properties. *J. Med. Chem.* **2013**, *56*, 3456−3466.

(29) Kasinski, A. L.; Du, Y.; Thomas, S. L.; Zhao, J.; Sun, S. Y.; Khuri, F. R.; Wang, C. Y.; Shoji, M.; Sun, A.; Snyder, J. P.; Liotta, D.; Fu, H. Inhibition of IkappaB kinase-nuclear factor-kappaB signaling pathway by 3,5-bis(2-flurobenzylidene)piperidin-4-one (EF24), a novel mono-ketone analog of curcumin. *Mol. Pharmacol.* **2008**, *74*, 654−661.

(30) Thomas, S. L.; Zhao, J.; Li, Z.; Lou, B.; Du, Y.; Purcell, J.; Snyder, J. P.; Khuri, F. R.; Liotta, D.; Fu, H. Activation of the p38 pathway by a novel monoketone curcumin analog, EF24, suggests a potential combination strategy. *Biochem. Pharmacol.* **2010**, *80*, 1309−1316.

(31) Olivera, A.; Moore, T. W.; Hu, F.; Brown, A. P.; Sun, A.; Liotta, D. C.; Snyder, J. P.; Yoon, Y.; Shim, H.; Marcus, A. I.; Miller, A. H.; Pace, T. W. Inhibition of the NF-kappaB signaling pathway by the curcumin analog, 3,5-bis(2-pyridinylmethylene)-4-piperidone (EF31): anti-inflammatory and anti-cancer properties. *Int. Immuno-pharmacol.* **2012**, *12*, 368−377.

(32) Lanotte, M.; Martin-Thouvein, V.; Najman, S.; Balerini, P.; Valensi, F.; Berger, R. NB4, a maturation inducible cell line with t(15;17) marker isolated from a human acute promyelocytic leukemia (M3). *Blood* **1991**, *77*, 1080−1086.

(33) Nason-Burchenal, K.; Maerz, W.; Albanell, J.; Allopenna, J.; Martin, P.; Moore, M. A.; Dmitrovsky, E. Common defects of different retinoic acid resistant promyelocytic leukemia cells are persistent telomerase activity and nuclear body disorganization. *Differentiation* **1997**, *61*, 321−311.

(34) Liang, G.; Shao, L.; Wang, Y.; Zhao, C.; Chu, Y.; Xiao, J.; Zhao, Y.; Li, X.; Yang, S. Exploration and synthesis of curcumin analogues with improved structural stability both in vitro and in vivo as cytotoxic agents. *Bioorg. Med. Chem.* **2009**, *17*, 2623−2631.

(35) Hasima, N.; Aggarwal, B. B. Targeting proteasomal pathways by dietary curcumin for cancer prevention and treatment. *Curr. Med. Chem.* **2014**, *21*, 1583−1594.

(36) MacManus, J. P.; Brewer, L. M.; Whitfield, J. F. The widely-distributed tumor protein, oncomodulin, is a normal constituent of human and rodent placentas. *Cancer Lett.* **1985**, *27*, 145−151.

(37) Balakrishnan, M. P.; Cilenti, L.; Ambivero, C.; Goto, Y.; Takata, M.; Turkson, J.; Li, X. S.; Zervos, A. S. THAP5 is a DNA-binding transcriptional repressor that is regulated in melanoma cells during

DNA damage-induced cell death. *Biochem. Biophys. Res. Commun.* **2011**, *404*, 195−200.

(38) Wang, X.; Thomas, B.; Sachdeva, R.; Arterburn, L.; Frye, L.; Hatcher, P. G.; Cornwell, D. G.; Ma, J. Mechanism of arylating quinone toxicity involving Michael adduct formation and induction of endoplasmic reticulum stress. *Proc. Natl. Acad. Sci. U.S.A.* **2006**, *103*, 3604−3609.

(39) Avonto, C.; Taglialatela-Scafati, O.; Pollastro, F.; Minassi, A.; Di Marzo, V.; De Petrocellis, L.; Appendino, G. An NMR spectroscopic method to identify and classify thiol-trapping agents: revival of Michael acceptors for drug discovery? *Angew. Chem., Int. Ed.* **2011**, *50*, 467−471.

(40) Milacic, V.; Banerjee, S.; Landis-Piwowar, K. R.; Sarkar, F. H.; Majumdar, A. P. N.; Dou, Q. P. Curcumin inhibits the proteasomal activity in human colon cancer cells in vitro and in vivo. *Cancer Res.* **2008**, *68*, 7283−7292.

(41) Unno, M.; Mizushima, T.; Morimoto, Y.; Tomisugi, Y.; Tanaka, K.; Yasuoka, N.; Tsukihara, T. The structure of the mammalian 20S proteasome at 2.75 Å resolution. *Structure* **2002**, *10*, 609−618.

(42) Adams, B.; Ferstl, E.; Davis, M.; Herold, M.; Kurtkaya, S.; Camalier, R.; Hollingshead, M.; Kaur, G.; Sausville, E.; Rickles, F. Synthesis and biological evaluation of novel curcumin analogs as anti-cancer and anti-angiogenesis agents. *Bioorg. Med. Chem.* **2004**, *12*, 3871−3883.

(43) Wang, Y.; Xiao, J.; Zhou, H.; Yang, S.; Wu, X.; Jiang, C.; Zhao, Y.; Liang, D.; Li, X.; Liang, G. A novel monocarbonyl analogue of curcumin, (1*E*,4*E*)-1,5-bis(2,3-dimethoxyphenyl)penta-1,4-dien-3-one, induced cancer cell H460 apoptosis via activation of endoplasmic reticulum stress signaling pathway. *J. Med. Chem.* **2011**, *54*, 3768−3778.

(44) Verdonk, M. L.; Cole, J. C.; Hartshorn, M. J.; Murray, C. W.; Taylor, R. D. Improved protein−ligand docking using GOLD. *Proteins* **2003**, *52*, 609−623.